Research Square

Preprints are preliminary reports that have not undergone peer review.
They should not be considered conclusive, used to inform clinical practice,
or referenced by the media as validated information.

Phase decomposition and dynamic modeling of the transient impact process in percussive drilling

Weihang Xi
University of Science and Technology Beijing
Songyuan Wang
University of Science and Technology Beijing
Xiang Tian
Jiangxi Siton Machinery Manufacturing Co., Ltd
Lulu Gao
gaolulu@ustb.edu.cn
University of Science and Technology Beijing
Fei Ma
University of Science and Technology Beijing

Research Article

Keywords: Hydraulic rock drill, Impact process, Phase decomposition, Dynamic modelling, Laser displacement sensor

Posted Date: November 24th, 2026

DOI: https://doi.org/10.21203/rs.3.rs-11670966/v1

License: This work is licensed under a Creative Commons Attribution 4.0 International License.
Read Full License

Additional Declarations: No competing interests reported.

Phase decomposition and dynamic modeling of the transient impact process in percussive drilling

Weihang Xi[a], Songyuan Wang[a], Xiang Tian[b], Lulu Gao[a,1], Fei Ma[a]

[a] *School of Mechanical Engineering, University of Science and Technology Beijing, Beijing 100083, China*

[b] *Jiangxi Siton Machinery Manufacturing Co., Ltd, Pingxiang 337009, China*

Abstract: The interaction between the piston and the load during the impact process governs the generation and propagation of stress waves. Analysis of stress has established that the impact process consists of multiple phases, but identifying these phases from measured piston displacement signals remains a challenge. To address this gap, this paper proposes a phase decomposition and dynamic modeling method for the transient impact process in percussive drilling, taking a hydraulic rock drill as a typical application scenario. The method employs jerk-based analysis to identify the phase boundaries from the measured piston displacement and establishes phase-specific dynamic models using the wave equation for the transient phase and the spring-mass equation for the compression and rebound phases. The proposed method is validated under three operating pressures using both kinematic measurements and independent pressure signals. The velocity error is within 6.9%~8.5% under the lower stiffness condition and 0.9% under the higher stiffness condition, with a maximum penetration error of around 2%. Pressure-based validation confirms the accuracy of impact onset detection, with a deviation of less than 0.2 ms from theoretical values. Based on the model, the energy transfer is analyzed, and the secondary impact is examined. The detachment position relative to the maximum compression position is identified as the governing factor of the secondary impact intensity, and the thrust force is identified as a tuning parameter for mitigating secondary impact and reducing the fatigue loading on the piston and seal components. In summary, this study provides an experimental identification of the phase structure of the impact process and offers insights into the phase-resolved energy partitioning under percussive loading.

Keywords: Hydraulic rock drill; Impact process; Phase decomposition; Dynamic modelling; Laser displacement sensor

1 Introduction

The impact process, in which a piston strikes a rod and transfers momentum and energy through stress wave propagation, is a fundamental problem in impact mechanics. Understanding the transient dynamic response of the piston–rod system under impact loading is therefore essential for characterizing the generation and propagation of stress waves. Such impact systems are widely used in percussive drilling, where this process is critical to improving drilling efficiency [1-4]. The acquisition and analysis of the impact process have therefore long been a central focus of research in this field.

Current research on the impact process mainly focuses on two aspects: the initial state of impact (i.e., the instantaneous velocity of the piston as it strikes the shank) and the post-impact propagation of stress waves. The former is typically addressed by system-level modeling, which predicts the pre-impact velocity of the impact piston based on the structural parameters of the rock drill. Gorodilov [5] proposed a simplified mathematical description of the impact piston motion during valve switching, which, however, resulted in relatively large deviations. Subsequently, Yang [6] and Hu [7] developed a complete rock drill model using AMEsim, which was further refined by Ma [8] to achieve high prediction accuracy. However, these system-level studies focused primarily on the pre-impact velocity of the piston, and the phase structure of the piston motion after impact was not addressed. On the stress wave side, research has been extensively developed both theoretically and experimentally. On the theoretical side, Lundberg and Collet [9] investigated the optimal wave shape for energy transfer efficiency, Lundberg, Rastemo and Huo [10] examined the effect of pre-impact waves on the coefficient of restitution. On the application side, Zhao [11] established a loading–unloading principle for impact dynamics through investigation of stress waveforms, Hashiba [12] constructed force-penetration curves based on stress wave measurements, and Zhang [13] established a quantitative link between stress wave frequency and rock fragmentation efficiency. In practice, Zheng [14] and Huo [15] improved percussive drilling equipment based on one-dimensional stress wave analysis. Other studies have revealed coupling effects between axial and torsional vibrations [16] or examined the correlation between stress waves and impact responses of concrete beams [17,18]. Taken together, these studies have

[1] Corresponding author.

Email address: gaolulu@ustb.edu.cn

revealed that the impact process involves multiple stages, including stress wave propagation, compression, and rebound.

Decomposing the piston motion from the stress side and decomposing it directly from the piston motion are two different paths. The analysis of stress has established the phase structure of the impact process through theoretical and numerical studies but identifying these phases from measured piston displacement signals remains a challenge. This is not because the importance of such a method has been overlooked, but because the measurement and analysis of the piston motion itself during impact remains a practical difficulty.

This difficulty is mainly attributable to the limitations of measurement and analysis techniques. Based on sensor installation and measurement parameters, these techniques fall into four categories. The first, contact direct measurement (e.g., electromagnetic method [19]), directly acquires piston motion but compromises sensor longevity and precludes testing under actual operating conditions. The second, contact indirect measurement represented by the stress wave method [20-22], evaluates impact performance without direct piston measurement and offers advantages in studying rock fragmentation [23-25]. However, strain gauges are fragile and highly sensitive to placement, limiting test duration and stability [26]. The third, non-contact direct measurement exemplified by laser displacement sensing [27], avoids sensor durability issues but it is limited to laboratory conditions due to the need for direct piston measurement. The fourth, non-contact indirect measurement based on acoustic signals [28-30], circumvents both durability and direct measurement constraints but fails to directly capture piston motion information. Consequently, among the four categories, the non-contact direct method represented by laser displacement sensing is the most suitable approach for investigating the impact process. However, there is still a gap between the obtained laser displacement data and uncovering the transient impact process.

To fill this gap, this paper proposes a phase decomposition and dynamic modeling method for the transient impact dynamics in percussive drilling. The method employs jerk-based analysis to decompose the impact process into five distinct phases and establishes phase-specific dynamic models, incorporating the wave equation for the transient phase and the spring-mass equation for the compression and rebound phases. The proposed model is validated under different operating pressures and load stiffness conditions using both kinematic measurements and independent pressure signals, with prediction errors within acceptable limits. Based on this model, the energy allocation during the impact process and the rebound collision phenomenon are analyzed. The contributions are summarized as follows:

(1) A threshold-free jerk-based decomposition method is proposed to identify the phase boundaries of the impact process directly from measured piston displacement, and the identified boundaries are combined with established phase-specific models to reconstruct the impact transient;

(2) Based on the model, the energy partitioning between the transient impact phase and the subsequent compression phase is calculated directly from the measured piston displacement, and the influence of load stiffness on this partitioning is analyzed;

(3) The secondary impact mechanism is analyzed, showing that the thrust force is a tuning parameter for mitigating secondary impact and reducing the fatigue loading on the piston and seal components.

The remainder of this paper is organized as follows. Section 2 discusses the limitations of current measurement techniques in capturing the impact process, then presents the framework of the proposed method and describes the detailed procedure of the phase decomposition method accordingly. Section 3 validates the decomposition results from two perspectives, namely kinematic parameters and internal and external pressure measurements, and discusses the impact process based on the model. Section 4 discusses the influence of load stiffness on energy partitioning and the mechanism of secondary impact. Section 5 summarizes the paper.

2 Experimental and modelling Methodology

2.1 Problem description

As discussed in the introduction, current research on hydraulic rock drills primarily focuses on pre-impact velocity and post-impact load response, while the impact process itself remains largely unexplored. This research gap stems from two underlying issues. First, the piston motion during the impact transient is difficult to capture due to the limitations of existing measurement techniques. Second, even when such data are available, no systematic method exists to decompose

the transient process and establish phase-specific dynamic models.

Figure 1 shows typical piston displacement curve measured by a laser displacement sensor (LDS) during one impact cycle. Based on the structural characteristics of the rock drill, the impact point can be directly identified in the figure. At this point, the displacement curve is divided into two parts. The part below the impact point represents the normal stroke of the piston, which is the focus of system-level modeling. The part above the impact point represents the piston motion after striking the shank. Compared with the monotonic linear variation of the normal stroke, this part exhibits typical nonlinear characteristics. However, without a systematic decomposition method, the underlying dynamic behavior of this nonlinear process cannot be quantitatively analyzed.

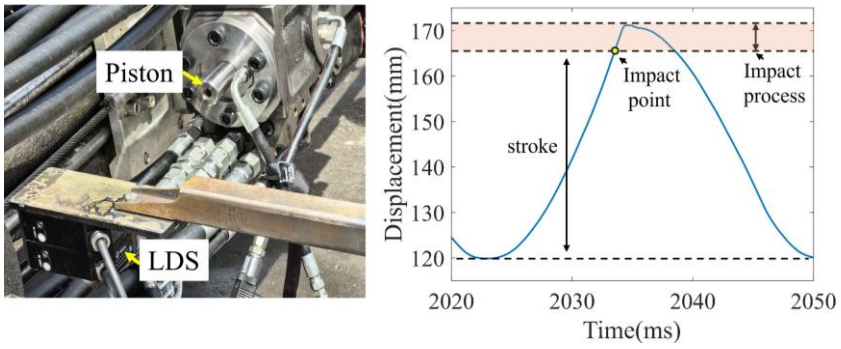


Figure 1 Measurement of the piston displacement using the LDS

2.2 Framework of the proposed data-driven decomposition and modeling

The proposed experimental-based modeling method for the impact process is illustrated in Figure 2. The core logic of this approach is to first identify the phase boundaries of the impact process from experimental data, rather than relying on pre-assumed thresholds or model-based segmentation. Once the phases are identified, the governing equations for each phase are selected according to the physical characteristics of that phase, drawing on established mechanical principles. In this way, the phase decomposition determines where each model applies, while the models themselves are based on well-established theory. The overall framework consists of three sequential steps.

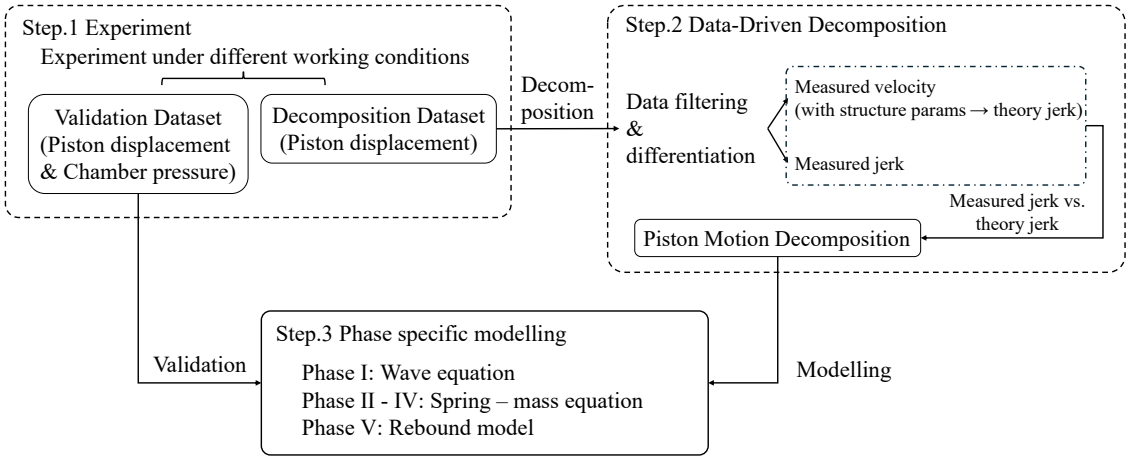


Figure 2 Framework of the data-driven decomposition and modeling method

The first step is preliminary experiments. Two types of data are synchronously collected on the test bench: the axial displacement waveform of the piston measured by a laser displacement sensor, and the pressure variations in the chambers of the percussive drill measured by pressure sensors.

The second step is time-domain localization and decomposition of the impact process. Based on the acquired pressure and piston displacement data, the time-domain localization of the impact process is achieved. Furthermore, through force analysis, the impact process is decomposed into several characteristic phases.

The third step is phase-specific modeling. Using the located impact process window as a reference, the impact

transient is further divided into several characteristic phases. The standard wave equation is employed to describe the stress wave propagation during the initial phase of impact. The forced vibration equation is then used to characterize the subsequent motion of the piston-bit system. These phase-specific models are connected through boundary conditions to form a complete predictive model of the impact process.

2.3 Experimental Setup

To obtain the piston motion and internal pressure parameters of the percussive drill during the impact process, while ensuring stable and adjustable load conditions, a percussive drill impact test bench is constructed.

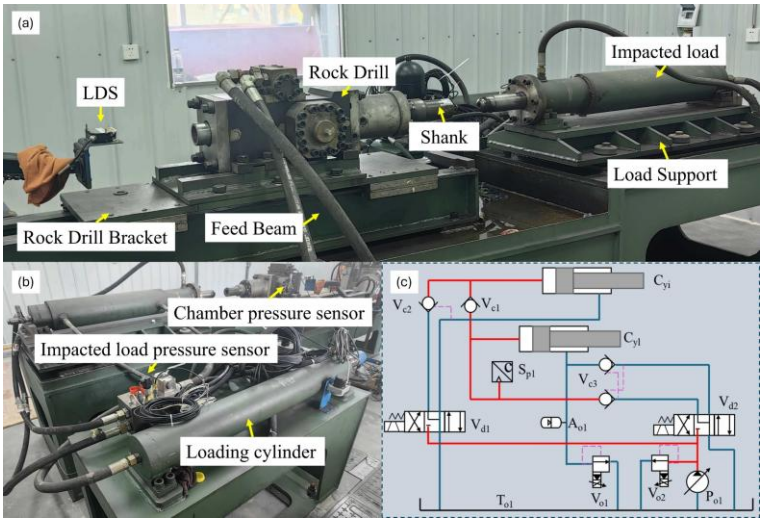


Figure 3 Rock drill impact test bench

Figure 3(a) shows the impact system consisting of the rock drill and the impacted cylinder. The rock drill is connected to the impacted cylinder through the shank. A feed beam provides the advancing force for the rock drill. A laser displacement sensor is installed at the rear end of the piston to measure its motion.

Figure 3(b) depicts the load adjustment section. The load magnitude is determined by the pressure in the rodless chamber of the impacted cylinder, which is controlled by a loading cylinder connected to it (specific hydraulic control method is shown in (c)). Pressure sensors are used to measure both the chamber pressure of the impacted cylinder and the chamber pressure of the rock drill. And all sensors used in the test bench are listed in Table 1.

Table 1 Sensors used in the bench

Sensor Type	Model	Range	Accuracy
LDS	optoNCDT 2300	0~200 mm	±0.1% FS
Pressure sensor	PTT-400	0~40 MPa	±0.5% FS

2.4 Data-driven phase decomposition of the impact process

From the experimental setup, accurate measurements of the piston displacement and chamber pressure are obtained. Based on data acquired from the experiment, this section presents a novel method for analyzing the impact process. The proposed method uses pressure signals to precisely locate the Impact Onset Moment (IOM) and the Detachment Onset Moment (DOM), thereby further decomposing the impact process into distinct phases.

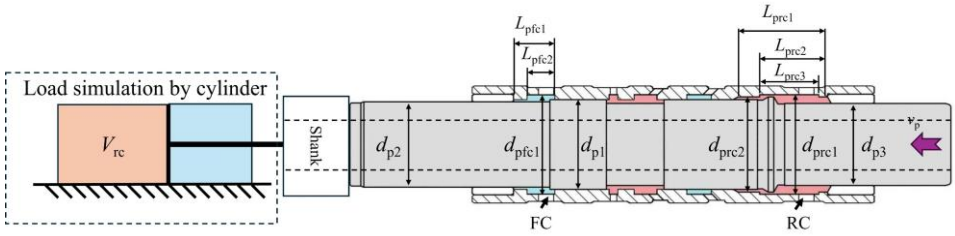


Figure 4 Schematic diagram of the impact piston and cylinder of the rock drill

As shown in Figure 4, the equation of the impact piston motion x_p is given by Eq.(1)

$$m_p \frac{d^2 x_p}{dt^2} = F_{pr} - F_{pf} - F_r \tag{1}$$

where m_p denotes the mass of the impact piston, F_{pr} the rear chamber hydraulic force, F_{pf} the front chamber hydraulic force, and F_r the contact load.

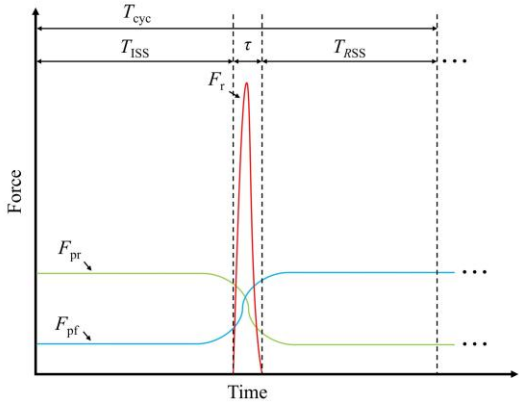


Figure 5 Force diagram of the piston during one impact cycle

And as illustrated in Figure 5, a complete impact cycle T_{cyc} is segmented into three stages based on the piston's force: the impact stroke T_{ISS}, the impact stage τ, and the return stroke T_{RSS}. The τ corresponds precisely to the period during which the contact reaction force F_r is present. Therefore, accurate determination of this stage is of critical importance for the analysis of the impact process.

However, direct determination of the impact stage based on force variation or piston acceleration presents several challenges.

(1) The contact reaction force F_r cannot be measured directly without intrusive sensors (e.g., strain gauges or piezoelectric force sensors), which are prone to damage under high-intensity percussive impacts;

(2) Though acceleration can reflect the onset of contact through a sudden change, the magnitude of this change varies with impact intensity, making it difficult to establish a universal threshold for detecting both the start and the end of the impact stage;

(3) Both the driving force and the chamber resistance also vary slowly during the impact cycle, and their derivatives contribute to the acceleration signal as low-frequency components, which may interfere with the identification of the transient impact features.

In summary, this paper proposes to use piston jerk as a reference indicator, leveraging the time-varying characteristics of forces to separate slowly varying components, thereby achieving a more accurate division of the impact process.

The following Eq.(2) to Eq.(4) are the expressions of the chamber hydraulic forces and the load acting on the piston.

$$F_{pr} = \pi p_r \left(d_{p1}^2 - d_{p3}^2 \right) / 4 \tag{2}$$

$$F_{\mathrm{pf}} = \pi p_{\mathrm{f}} \left(d_{\mathrm{p1}}^2 - d_{\mathrm{p2}}^2 \right) / 4 \tag{3}$$

$$F_{\mathrm{r}} = \begin{cases} F_{\mathrm{r}} & x_{\mathrm{p}} \le 0 \\ 0 & x_{\mathrm{p}} > 0 \end{cases} \tag{4}$$

The expression for the piston jerk J_{p} is obtained by substituting Eq.(2) ~ Eq.(4) into Eq.(1) and then differentiating, as shown in Eq.(5).

$$m_{\mathrm{p}} J_{\mathrm{p}} = \begin{cases} \dfrac{\pi}{4}\left(d_{\mathrm{p1}}^2 - d_{\mathrm{p3}}^2 \right) \dfrac{\mathrm{d}p_{\mathrm{r}}}{\mathrm{d}t} - \dfrac{\pi}{4}\left(d_{\mathrm{p1}}^2 - d_{\mathrm{p2}}^2 \right) \dfrac{\mathrm{d}p_{\mathrm{f}}}{\mathrm{d}t} - \dfrac{\mathrm{d}F_{\mathrm{r}}}{\mathrm{d}x} \dfrac{\mathrm{d}x}{\mathrm{d}t} & x_{\mathrm{p}} \le 0 \\ \dfrac{\pi}{4}\left(d_{\mathrm{p1}}^2 - d_{\mathrm{p3}}^2 \right) \dfrac{\mathrm{d}p_{\mathrm{r}}}{\mathrm{d}t} - \dfrac{\pi}{4}\left(d_{\mathrm{p1}}^2 - d_{\mathrm{p2}}^2 \right) \dfrac{\mathrm{d}p_{\mathrm{f}}}{\mathrm{d}t} & x_{\mathrm{p}} > 0 \end{cases} \tag{5}$$

Eq.(5) indicates that the piston jerk during the impact process is influenced by both hydraulic forces and the impact force. To isolate the effect of the impact force, the pressure variation must be evaluated. Therefore, as illustrated in Figure 4, since the present study focuses primarily on the piston motion within a short time window around the impact event, the moment when the piston contacts the bit is taken as the reference position. At this reference position, the effective volumes of the front and rear chambers can be obtained from Eq.(6) ~ Eq.(7)

$$V_{\mathrm{pr}} = \pi \left(d_{\mathrm{p1}}^2 - d_{\mathrm{p3}}^2 \right) \left(L_{\mathrm{re}} + x_{\mathrm{p}} \right) / 4 \tag{6}$$

$$V_{\mathrm{pf}} = \pi \left(d_{\mathrm{p1}}^2 - d_{\mathrm{p2}}^2 \right) \left(L_{\mathrm{fe}} - x_{\mathrm{p}} \right) / 4 \tag{7}$$

where L_{re} and L_{fe} are the equivalent lengths, calculated by Eq.(8) and Eq.(9).

$$L_{\mathrm{re}} = L_{\mathrm{prc1}} \left(d_{\mathrm{prc2}}^2 - d_2^2 \right) / \left(d_{\mathrm{p1}}^2 - d_{\mathrm{p3}}^2 \right) + L_{\mathrm{prc2}} + L_{\mathrm{prc3}} \left(d_{\mathrm{prc1}}^2 - d_{\mathrm{p3}}^2 \right) / \left(d_{\mathrm{p1}}^2 - d_{\mathrm{p3}}^2 \right) \tag{8}$$

$$L_{\mathrm{fe}} = L_{\mathrm{pfc1}} + L_{\mathrm{pfc2}} \left(d_{\mathrm{pfc1}}^2 - d_{\mathrm{p1}}^2 \right) / \left(d_{\mathrm{p1}}^2 - d_{\mathrm{p2}}^2 \right) \tag{9}$$

From the effective volume, the relationship between the pressure rate of change and the piston velocity can be derived, as shown in Eq.(10) and Eq.(11).

$$\mathrm{d}p_{\mathrm{pr}} / \mathrm{d}t = \pi E_{\mathrm{o}} \left(d_{\mathrm{p1}}^2 - d_{\mathrm{p3}}^2 \right) \dot{x}_{\mathrm{p}} / 4 V_{\mathrm{pr}} \tag{10}$$

$$\mathrm{d}p_{\mathrm{pf}} / \mathrm{d}t = \pi E_{\mathrm{o}} \left(d_{\mathrm{p1}}^2 - d_{\mathrm{p2}}^2 \right) \dot{x}_{\mathrm{p}} / 4 V_{\mathrm{pf}} \tag{11}$$

By substituting Eq.(6) ~ Eq.(11) into Eq.(5), the J_{p} can be expressed in terms of piston velocity and displacement, leading to Eq.(12)

$$J_{\mathrm{p}} = \begin{cases} \dfrac{E_{\mathrm{o}} \left(A_{\mathrm{re}} L_{\mathrm{fe}} - A_{\mathrm{fe}} L_{\mathrm{re}} - A_{\mathrm{fe}} x_{\mathrm{p}} - A_{\mathrm{re}} x_{\mathrm{p}} \right)}{m_{\mathrm{p}} \left(L_{\mathrm{re}} + x_{\mathrm{p}} \right) \left(L_{\mathrm{fe}} - x_{\mathrm{p}} \right)} \dot{x}_{\mathrm{p}} - \dfrac{\mathrm{d}F_{\mathrm{r}}}{\mathrm{d}x} \dfrac{\mathrm{d}x}{\mathrm{d}t} & x_{\mathrm{p}} \le 0 \\ \dfrac{E_{\mathrm{o}} \left(A_{\mathrm{re}} L_{\mathrm{fe}} - A_{\mathrm{fe}} L_{\mathrm{re}} - A_{\mathrm{fe}} x_{\mathrm{p}} - A_{\mathrm{re}} x_{\mathrm{p}} \right)}{m_{\mathrm{p}} \left(L_{\mathrm{re}} + x_{\mathrm{p}} \right) \left(L_{\mathrm{fe}} - x_{\mathrm{p}} \right)} \dot{x}_{\mathrm{p}} & x_{\mathrm{p}} > 0 \end{cases} \tag{12}$$

where $A_{\mathrm{re}} = \pi \left(d_{\mathrm{p1}}^2 - d_{\mathrm{p3}}^2 \right) / 4$ is the effective area of the impact piston rear chamber, and $A_{\mathrm{fe}} = \pi \left(d_{\mathrm{p1}}^2 - d_{\mathrm{p2}}^2 \right) / 4$ is the

effective area of the impact piston front chamber.

The jerk expression in Eq.(12) suppresses the slowly varying contribution of the driving chamber pressure through differentiation. Furthermore, it expresses the impact-related terms in terms of piston velocity and displacement, both of which are reliably measurable quantities. This eliminates the need for a universal threshold that would otherwise be required when using acceleration directly, providing a solid foundation for identifying the impact process.

With the IOM taken as the reference position, the piston displacement is approximately zero during the impact process. Therefore, the slowly varying component of the piston jerk is approximately proportional to the piston velocity via a coefficient k_{cp}, which is determined by the cylinder–piston structure, as given in Eq.(13).

$$k_{cp} = \frac{E_o \left(A_{re} L_{re} - A_{fe} L_{fe} \right)}{m_p L_{re} L_{fe}} \tag{13}$$

The piston displacement was measured using the laser displacement sensor at a sampling frequency of 10 kHz. A low-pass filter with a cutoff frequency of 600 Hz was applied to the displacement signal before differentiation. The cutoff frequency was selected based on the Fourier spectrum of the measured displacement: the resonance peak associated with the impact frequency (40 Hz in the present experiments) is preserved, while high-frequency measurement noise is suppressed. The cutoff frequency may be adjusted for different impact frequencies according to the same criterion. The jerk was then computed using the central difference method.

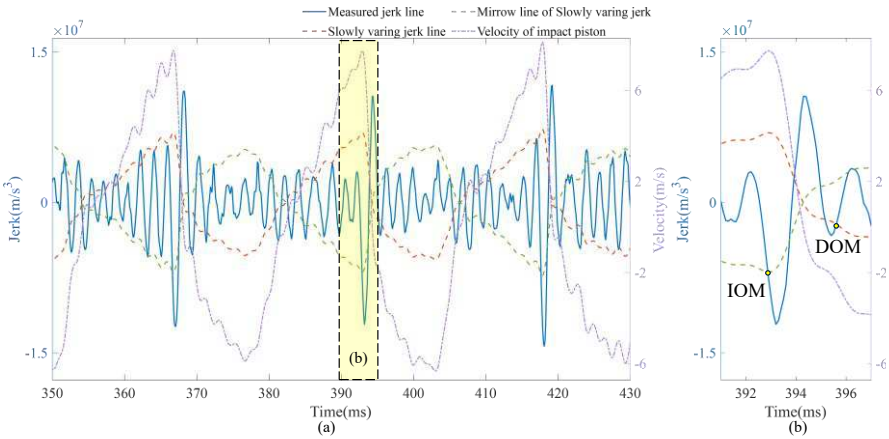


Figure 6 Determination of IOM and DOM using jerk envelopes

The slowly varying component of the piston jerk is given by $j_{slow} = k_{cp} v_p$. The piston velocity v_p changes sign during the impact process. Therefore, j_{slow} exhibits opposite polarities on the two sides of the impact. To unify these opposite-polarity features into a single detection framework, the mirror line of j_{slow} is taken. As shown in Figure 6 (a), the original curve and its mirror together form a closed envelope that symmetrically bounds the impact process. Therefore, when the jerk calculated from the measured piston displacement exceeds the envelope, it indicates that the piston is subjected to an additional force beyond the chamber hydraulic forces. In the context of the impact process, this corresponds precisely to the onset of the contact force. Conversely, when the jerk falls back within the envelope, the piston motion returns to being dominated solely by hydraulic forces. As illustrated in Figure 6 (b), the first intersection where the measured jerk exceeds the envelope marks the IOM, and the last intersection where it returns within the envelope marks the DOM.

2.5 Phase-specific dynamic modeling

Based on the envelope analysis described in Section 2.4, the jerk curve of the impact process is obtained, as shown in Figure 7. The slowly varying envelope j_{slow} represents the jerk contribution from chamber hydraulic forces only, while the measured jerk includes the additional effect of the contact reaction force. Comparing the measured jerk with the slowly varying envelope reveals that the intersection points between them reflect the internal structure of the impact process.

Based on the characteristic points identified from the jerk and velocity curves, the impact process is divided into five

sequential phases:

- **Phase I** (Transient impact): from IOM to Equilibrium Onset Moment (EOM), where stress wave propagation dominates.
- **Phase II** (Uniform compression): from EOM to Direction Change Moment (DCM), where the piston and shank move together under uniform stress.
- **Phase III** (Decelerating compression): from DCM to Maximum Compression Moment (MCM), where the piston decelerates to zero velocity under reverse thrust.
- **Phase IV** (Rebound): from MCM to DOM or from MCM to IOM_2, where elastic recovery drives the piston backward.
- **Phase V** (Rebound impact): during rebound, where the piston may re-contact the shank, causing a secondary jerk peak.

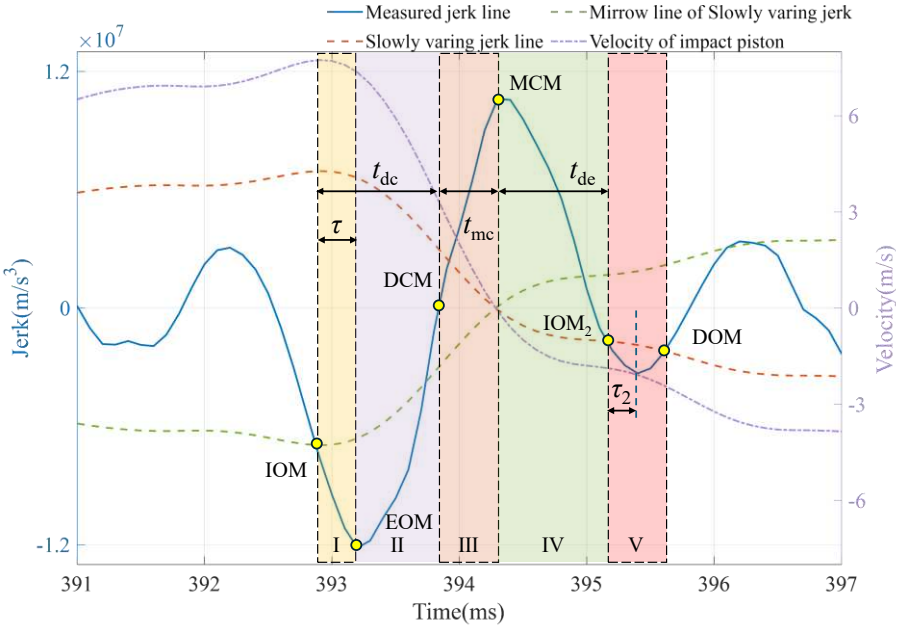


Figure 7 Data-driven decomposition of the impact process

To accurately reproduce the impact process, this section establishes phase-specific dynamic models corresponding to each of the five phases identified above. The proposed models adhere to the following assumptions:

(1) The stress wave propagates as a one-dimensional wave along the axial direction, neglecting transverse effects;

(2) Both the piston and shank materials remain linearly elastic and obey Hooke's law throughout the impact process;

(3) Damping effects are negligible across all five phases;

(4) The impact piston, shank and impacted piston are modeled as a uniform rod with constant wave speed;

(5) The impact interface is treated as an ideal planar contact;

In Phase I, the stress generated by impact requires a finite time to propagate through the piston and the load. Consequently, during the short period immediately after impact, the piston motion is governed by wave dynamics rather than rigid-body motion, while the influence of chamber pressure on the piston is negligible. Under these conditions, the one-dimensional wave equation [31] is adopted as the governing equation, from which the stress continuity and particle velocity continuity conditions at the impact interface are derived, as given in Eq.(14)

$$\begin{cases} A_{\mathrm{p}}\left(\sigma_{\mathrm{i}}+\sigma_{\mathrm{r}}\right)=-A_{\mathrm{s}}\sigma_{\mathrm{t}} \\ v_{\mathrm{i}}+v_{\mathrm{r}}=v_{\mathrm{t}} \end{cases} \tag{14}$$

where, σ_{i} and σ_{r} are the incident and reflect stress generated by the piston impact, respectively, σ_{t} is the transmitted stress propagating into the shank, v_{i}, v_{r} and v_{t} are the corresponding particle velocities, A_{p} is the cross-sectional area of the impact

interface, A_s is the cross-sectional area of the shank interface.

Based on the above assumptions, σ_t can be determined by $\sigma_t = -k_L x_p/A_s$ and the particle velocities are given by $v_i = \sigma_i/z_p$, $v_r = \sigma_r/z_p$, $v_t = \sigma_t/z_s$. With the area ratio defined as $R = A_p/A_s$, the governing equation for the impact phase is obtained as Eq.(15)

$$\dot{x}_{p1} + \frac{Rk_L}{z_p A_p} x_{p1} = 2\frac{\sigma_i}{z_p} \tag{15}$$

where the $z_p = \rho_p c_p$ is the impedance of the piston, z_s is the impedance of the shank. Since the piston, shank, and impacted piston are made of similar materials, it is reasonable to assume $z_p = z_s$, for simplification.

Based on Eq.(14), σ_i can be defined as Eq.(16)

$$\sigma_i = v_{pi} z_p \tag{16}$$

where v_{pi} is the impact velocity.

Assuming the piston stiffness is significantly greater than that of the load side, the compressive displacement can be considered equivalent to the piston displacement. Therefore, the displacement of the impact piston is given by Eq.(17)

$$x_{p1} = \frac{v_{pi}}{R\beta}\left(1 - e^{-R\beta t}\right) \tag{17}$$

where $\beta = k_L/(z_p A_p)$ is the eigenvalue of the impact system.

Analysis of the transient impact duration τ in Figure 7 reveals that it exactly equals the round-trip time of the stress wave along the load side, as shown in Eq(18)

$$\tau = 2L_r/c_r \tag{18}$$

where the L_r is farthest propagation distance of the stress wave within the uniform impedance rod, and c_r is the wave velocity in the rod.

In Phase II, following the uniform distribution of stress, the piston and shank move together at the same velocity. The gradual decrease of the jerk from its peak value to zero is jointly determined by the increase of load force with compression and the decrease of hydraulic thrust. The zero-crossing of the jerk marks the moment when the resultant hydraulic force changes direction due to the switching of the directional valve. Accordingly, piston motion during this phase is governed by Eq.(19)

$$\left(m_p + m_s + m_r\right)\ddot{x}_{p2} + k_L x_{p2} = F_{pi} \tag{19}$$

where m_p is the impact piston mass, m_s the shank mass, m_r the impacted piston mass, and F_{pi} the resultant hydraulic force during impact stroke of the hydraulic rock drill.

For an ideal rock drill design, the directional valve is typically actuated to switch immediately after IOM. Therefore, the termination time of the Phase II (t_{dc}) is determined by the switching timing of the valve, which can be expressed as a function of the design parameters, as given in Eq.(20)

$$t_{dc} = \left\{2L_v m_v \Big/ \left[p_{in}\left(A_{sig} - A_{in}\right)\right]\right\}^{1/2} \tag{20}$$

where, L_v is the valve switching distance, m_v is the mass of the valve, p_{in} is the input pressure, A_{sig} and A_{in} are effective area of the valve.

Define $M = m_p + m_s + m_r$, and $\omega = k_L/M$, solution of Eq.(19) is given by Eq.(21)

$$x_{\mathrm{p2}} = \left(x_{\mathrm{p1_end}} - F_{\mathrm{pi}}/k_{\mathrm{L}}\right)\cos\left(\omega t\right) + v_{\mathrm{p1_end}}\sin\left(\omega t\right)/\omega + F_{\mathrm{pi}}/k_{\mathrm{L}} \tag{21}$$

where $x_{\mathrm{p1_end}}$ is the final position of the impact piston in Phase I, and $v_{\mathrm{p1_end}}$ is the final velocity.

In Phase III, as the piston remains in the compression phase, it continues to compress the load until its velocity reaches zero. However, due to the reversal of the resultant hydraulic force caused by the switching of the directional valve, the equation of motion for the piston becomes Eq.(22)

$$\left(m_{\mathrm{p}} + m_{\mathrm{s}} + m_{\mathrm{r}}\right)\ddot{x}_{\mathrm{p3}} + k_{\mathrm{L}}x_{\mathrm{p3}} = -F_{\mathrm{pr}} \tag{22}$$

where F_{pr} is the resultant hydraulic force during return stroke.

Since Eq.(22) differs from Eq.(19) only in constant terms, the duration of this process t_{mc} can be directly obtained from the general solution given in Eq.(21), as shown in Eq.(23)

$$t_{\mathrm{mc}} = \omega^{-1}\arctan\left(v_{\mathrm{p2_end}}\left[\omega\left(x_{\mathrm{p2_end}} + F_{\mathrm{pr}}/k_{\mathrm{L}}\right)\right]^{-1}\right) \tag{23}$$

In Phase IV, the piston begins to rebound in the reverse direction, with its motion governed by Eq.(24). The degradation coefficient α is introduced to characterize the difference in k_{L} between the Phase I ~ III and Phase IV. This coefficient is analogous to the unloading parameter in the bilinear force–penetration model [32], where the loading and unloading stiffnesses are also described by two distinct slopes. In the present system, this stiffness variation is primarily attributed to the nonlinear behavior of the hydraulic system under alternating loads, including oil compressibility hysteresis and nonlinear friction response; and the compliance of seals and contact interfaces, which produce different deformation and recovery patterns between loading and unloading. Although the unloading stiffness differs from the loading stiffness, the rebound duration t_{de} is assumed to be approximately equal to the compression duration (the sum of Phases I, II, and III), given the weak damping and the linear elasticity assumption.

$$\left(m_{\mathrm{p}} + m_{\mathrm{s}} + m_{\mathrm{r}}\right)\ddot{x}_{\mathrm{p4}} + \alpha k_{\mathrm{L}}x_{\mathrm{p4}} = -F_{\mathrm{pr}} \tag{24}$$

Phase V is essentially a repetition of Phase I, with the key difference being that the load actively impacts the piston. Consequently, the duration of this phase is determined by the length of the piston, as given in Eq.(25). The piston motion during this phase follows a similar form to Eq.(17), except that the piston velocity is replaced by the impact velocity of the load.

$$\tau_2 = 2L_{\mathrm{p}}/c_{\mathrm{p}} \tag{25}$$

3 Validation

3.1 Numerical model setup

To validate the proposed model, the TFYY400 hydraulic rock drill is taken as an example. The model is verified from two aspects: kinematics and timing, corresponding to Sections 3.2 and 3.3, respectively. The specific geometric and material parameters are summarized in Table 2.

Table 2 Parameters used in the impact process model

Symbol	Description	value	unit
d_{p1}, d_{p2}, d_{p3}	diameter of impact piston	82, 78, 75	mm
d_{pfc1}, d_{prc1}, d_{prc2}	diameter of front/rear chamber	86, 90, 86	mm
m_{p}, m_{v}, m_{s}, m_{r}	mass of impact piston/spool/shank/impacted piston	11.7, 0.35, 10, 35	kg

L_{pfc1}, L_{pfc2}	length of front chamber	38, 25.5	mm
L_{prc1}, L_{prc2}, L_{prc3}	length of rear chamber	87, 71.5, 61,5	mm
L_p, L_r	length of impact/impacted piston	355, 953	mm
A_p, A_s	impact area of impact piston/shank	2413, 5391	mm^2
A_{sig}, A_{in}	effective area of valve	220, 113	mm^2
ρ_p	density of piston material	9000	kg/m^3
c_p	wave velocity in material	4830.5	m/s
F_{tt}	thrust force of the hydraulic rock drill	15	kN

The axial stiffness of the load k_L can be calculated by Eq.(26), and its parameters are listed in Table 3.

$$k_L = E_o A_r^2 / V_{rc} \tag{26}$$

Table 3 Parameters of the impacted system

Symbol	Description	Value	Unit
E_o	effective modulus of the hydraulic oil	900	MPa
A_r	cap-side area of the impacted piston	1.227×10^{-2}	m^2
V_{rc}	cap-side chamber volume of the impacted cylinder	2.45, 1.84	L

Based on preliminary experimental data, the value of α is estimated to be in the range of 0.1 to 0.2 for the tested system. Therefore α = 0.15 is adopted in the following analysis. Besides, although Phase V is observed in preliminary experiments, it is not considered in the validation due to its limited influence on the piston kinematics and will be further analyzed in discussion part.

3.2 Validation against measured kinematics

To evaluate the reliability, stability, and generalizability of the proposed model, experimental tests are conducted under three different operating pressures (12 MPa, 14 MPa, and 16 MPa) and two different k_L (controlled by impacted system). In each test, the rock drill impacts the same impacted cylinder with identical system parameters. The piston motion is measured using a laser displacement sensor. The measured initial conditions are fed into the proposed model to generate predictions of the piston velocity and displacement. These predictions are then compared with the measured data to assess the model performance.

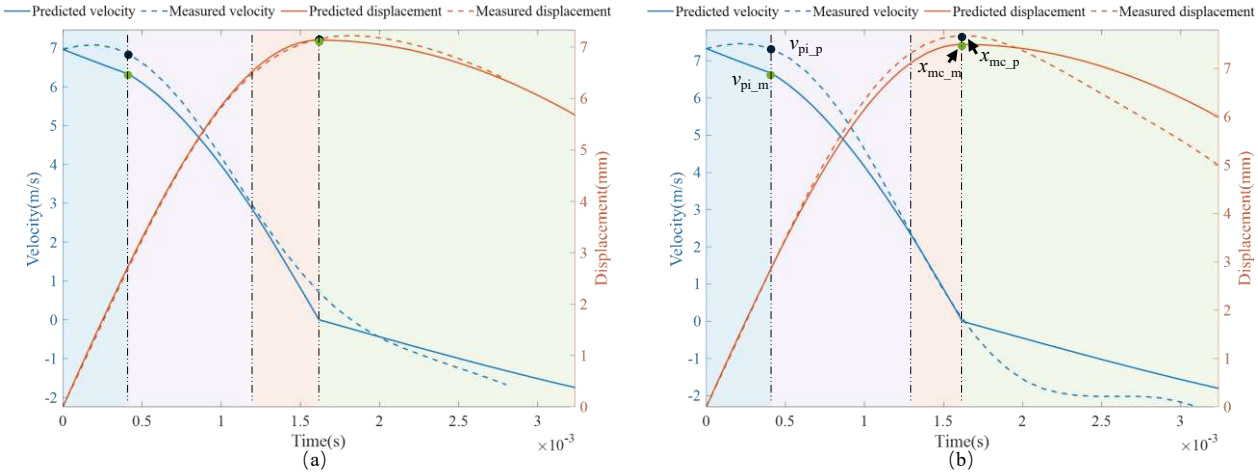


Figure 8 Comparison of predicted and measured kinematics: (a) p_{in} = 12MPa, V_{rc} = 2.45 L, (b) p_{in} = 14MPa, V_{rc} = 2.45 L

Figure 8 compares the predicted and measured impact process curves under different operating pressures (12 MPa and 14 MPa) with the same impacted system configuration (V_{rc} = 2.45 L). The piston velocity v_{pi} at the end of the Phase I and the maximum compression x_{mc} are selected as key metrics. For velocity, the measured decay is smaller than predicted, with errors of 6.9% and 8.5%, attributed to the relatively low impact velocity and soft load stiffness (due to the long oil column), which prevent full stress-wave dominance. For maximum compression, the errors are only 0.4% and 2.3%, as the effect of neglecting damping is suppressed over the longer timescale of rigid-body compression. Based on the above analysis, although the velocity prediction exhibits deviations ranging from 6.9% to 8.5% depending on the load conditions, the predicted maximum compression shows excellent agreement with the measured values under different operating pressures. Moreover, the predicted curves capture the overall trends of piston velocity and displacement with reasonable accuracy. Therefore, the reliability and stability of the proposed model is demonstrated.

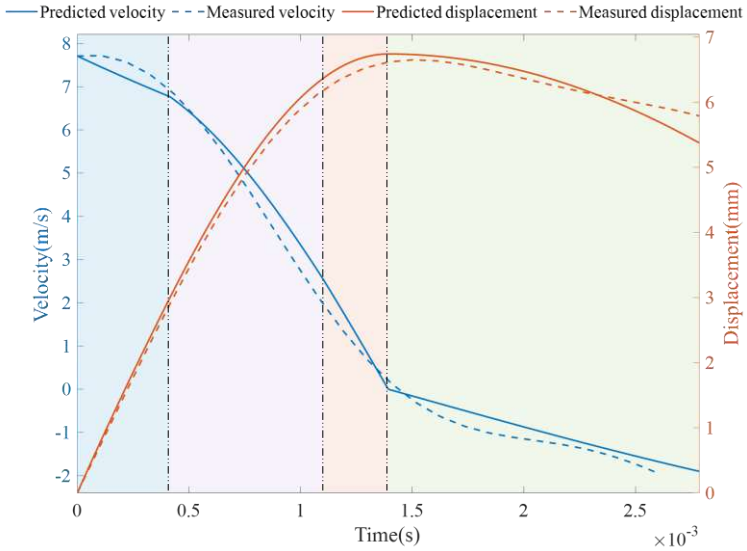


Figure 9 Comparison of predicted and measured kinematics (p_{in} = 16MPa, V_{rc} = 1.84 L)

To further verify the generalizability of the proposed model and to mitigate the issue of insignificant nonlinearity caused by low impact velocity and low load stiffness, the operating pressure is increased to 16 MPa, and V_{rc} is reduced to 1.84 L. The comparison curves under this condition are shown in Figure 9. Under this condition, both the initial piston velocity and the system stiffness increase significantly. The velocity deviation at the end of the transient impact phase reduces to 0.9%, and the maximum compression error is 1.8%. This improvement supports the model assumption that higher impact velocity and greater stiffness promote stress-wave-dominated behavior, under which the proposed model performs more accurately. This result also demonstrates the generalizability of the proposed model, as it accurately predicts

the impact process under a new set of operating and impacted system parameters without recalibration.

3.3 Validation against pressure-derived timing

In addition to kinematic validation, the proposed model is further verified by comparing the predicted timing of key impact events with those extracted from independently measured pressure signals. Specifically, two comparisons are conducted: the switching point is identified from the intersection of the front and rear chamber pressure curves of the rock drill; and the peak and pulse width of the impacted cylinder pressure are used to determine the impact onset and to validate the stress wave theory.

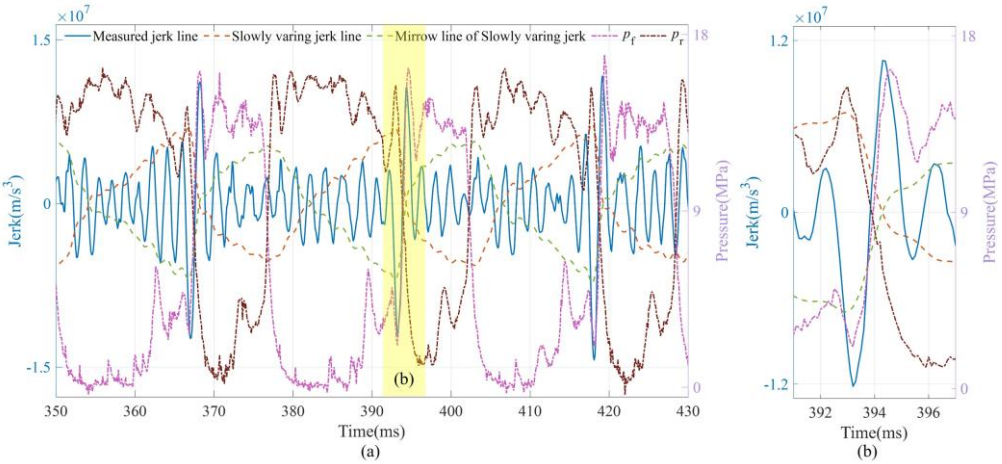


Figure 10 Comparison of the DCM identified from pressure crossover and the proposed method (p_{in} = 16MPa)

As shown in Figure 10 (a), the pressure curves of the front (p_f) and rear chambers (p_r) of the rock drill intersect at a distinct point, which allows easy determination of the valve switching completion timing. Observing Figure 10 (b), this pressure intersection point coincides closely with the zero-crossing of the piston jerk, which is the DCM defined by the proposed method. Comparing these two time points over multiple impact cycles, the time difference is consistently within ±0.1 ms, which is within the sampling frequency tolerance.

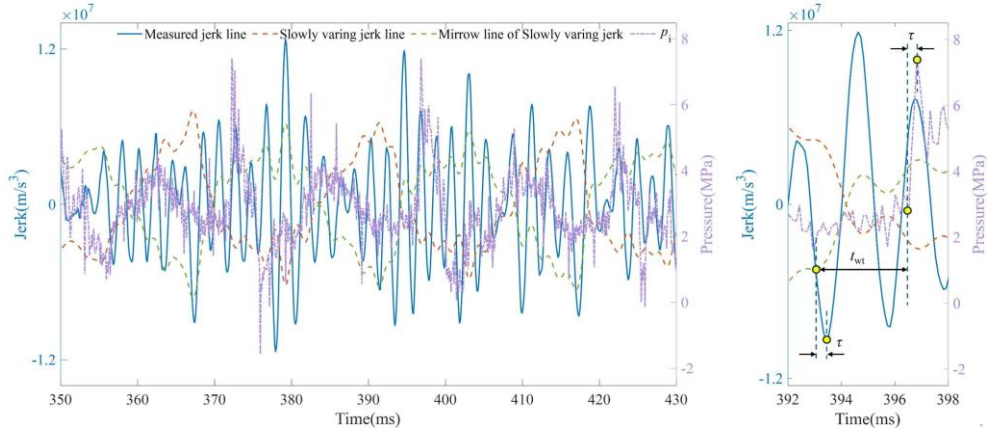


Figure 11 Comparison of the IOM identified from pressure of impacted cylinder and the proposed method (p_{in} = 16MPa)

As shown in Figure 11, which presents a separate set of experimental data with simultaneous measurement of piston motion and impacted cylinder pressure, the time interval between the impact onset identified by the proposed method and the onset of the pressure peak in the impacted cylinder is consistently around 4.7 ms across multiple cycles. Considering the propagation time of the stress wave through the piston and the hydraulic oil to reach the pressure sensor, this interval can be calculated theoretically using Eq.(27). The deviation between the measured interval and the theoretical value is within 0.2 ms, indicating that the impact onset derived from the pressure peak is consistent with that determined by the proposed method. Furthermore, the rise time of the marked impacted cylinder pressure peak coincides with the duration

of Phase I defined in this paper. This agreement provides independent experimental evidence that the stress wave propagation in Phase I directly governs the pressure buildup in the impacted cylinder, confirming the physical basis of the proposed phase decomposition.

$$t_{\mathrm{wt}} = L_{\mathrm{r}}/c_{\mathrm{r}} + L_{\mathrm{pipe}}/c_{\mathrm{o}} \tag{27}$$

where, L_{pipe} = 4 m is the length of the pipe connecting the impact cylinder to the valve block with pressure sensor.

4 Discussion

The validation results in Section 3 have demonstrated the predictive capability of the proposed model across different stiffness conditions. The following discussion provides a deeper analysis of the underlying mechanisms governing the observed behavior, focusing on the role of load stiffness in energy partitioning during the impact process and the condition and mechanism of secondary impact.

4.1 Influence of Load Stiffness on the Validity of the Wave-Dominated Assumption

From an energy perspective, the phase decomposition established in this study allows the energy flow during the impact process to be resolved into distinct phases. Previous studies have established the relationship between overall energy transfer efficiency and the load stiffness [33,34]. Based on this, the present work further analyzes the energy transfer on a phase-by-phase basis, decomposing it into two parts: the kinetic energy loss of the piston at the end of Phase I, which reflects the energy transferred to the load during the transient impact phase, and the compression displacement during Phases II–III, which reflects the energy consumed by compression before the maximum compression moment is reached.

Since the pressure in the impacted cylinder is held constant during the tests, the load stiffness is controlled primarily by the piston extension. Under this condition, the compression displacement of the impacted piston provides a direct measure of the energy used for forward penetration.

As shown in Table 4 the velocity variation during Phase I increases from 2.2% to 11.4% as the load stiffness increases from 5.4×10^7 N/m to 7.4×10^7 N/m. This indicates that a higher stiffness leads to a larger proportion of impact energy being transferred to deformation work during Phase I, consistent with the proposed two-stage framework. Correspondingly, the penetration during Phases II–III decreases from 4.6 mm to 3.2 mm, indicating that a smaller proportion of the energy is consumed by compression. These contrasting trends indicate that the way energy is distributed between the transient impact phase and the subsequent compression phase has a direct influence on penetration. This phase-resolved partitioning provides additional information that is not directly available from the overall efficiency analysis.

Table 4 Velocity variation at the end of Phase I under different stiffness conditions

Stiffness(N/m)	Impact velocity (m/s)	End-of-Phase I velocity (m/s)	Velocity variation	Penetration during Phases II–III (mm)
5.4×10^7	6.96	6.81	2.2%	4.6
7.4×10^7	7.71	6.83	11.4%	3.2

While Table 4 presents the experimental results under two representative stiffness conditions, Figure 12 extends the analysis to a broader range of stiffness and area ratio values. It presents the energy conversion during Phase I under varying stiffness k_{L} and area ratio R conditions, derived from Eq.(17) in Section 2.

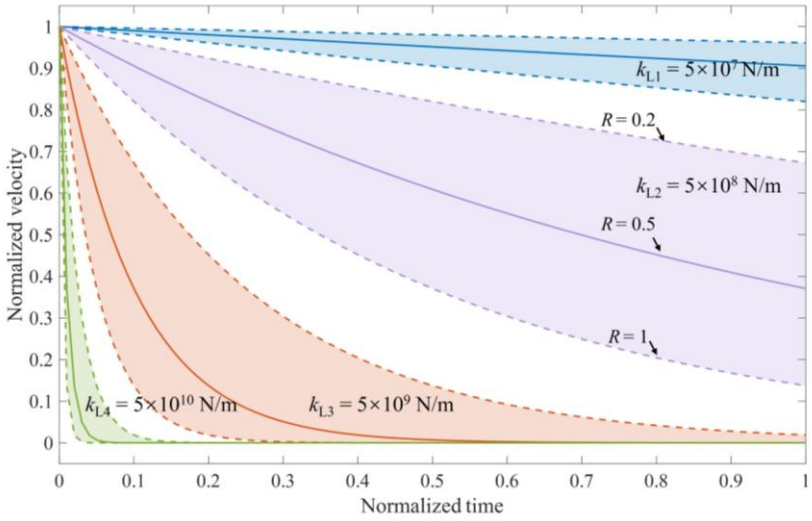


Figure 12 Normalized velocity under varying stiffness and area ratio

To better describe the influence of stiffness, the load stiffness can be classified into three ranges: soft load ($k_L < 5\times10^8$ N/m), transitional load (5×10^8 N/m $< k_L < 5\times10^9$ N/m) and hard load ($k_L > 5\times10^9$ N/m). Figure 12 illustrates how the velocity variation of the impact piston during Phase I depends on the system stiffness and the area ratio. Under soft load conditions, the velocity variation exhibits a nearly linear trend, and the area ratio has little influence. In the transitional range, the nonlinearity becomes increasingly pronounced, and the velocity variation is highly sensitive to the area ratio. Under hard load conditions, the velocity variation returns to a nearly linear trend, and the area ratio again has little effect. From an energy perspective, within one stress wave cycle, the maximum kinetic energy of the piston under soft load conditions is only about 32.8% of the input energy, whereas under hard load conditions it approaches nearly 100%. In the transitional range, the energy loss varies from 55.1% to 98.1%, depending on the area ratio.

The sensitivity of the energy conversion to the area ratio R varies significantly across different stiffness ranges. Under soft load conditions, the energy available for deformation is relatively small, making the influence of R less noticeable. Under hard load conditions, the energy transfer is too rapid and efficient for R to exert a measurable effect. It is only in the transitional range, where the energy of deformation constitutes a significant share of the total impact energy and the interaction lasts long enough, that the area ratio R exerts a dominant influence on energy conversion.

In summary, the analysis reveals that load stiffness acts as a controlling parameter in the two-stage energy allocation process. Higher stiffness promotes greater energy conversion in Phase I, whereas the influence of area ratio is most pronounced in the transitional range. This stiffness-dominated energy partitioning provides a mechanistic understanding of how impact energy is distributed between deformation and motion in percussive systems.

4.2 Condition and mechanism of secondary impact

The rebound stage (Phase IV) may be followed by a secondary impact between the piston and the load, corresponding to Phase V in the proposed phase decomposition. Although this event has limited effect on the piston velocity at IOM of the subsequent cycle under the tested conditions, the high-frequency vibrations it induces can adversely affect seal integrity and piston end durability in practical applications. After the primary impact and before the secondary impact, the front chamber undergoes a pressure switch as the directional valve changes to the return stroke. When the secondary impact occurs during this switching process, the mechanical impact adds to the already fluctuating chamber pressure, which can amplify the pressure oscillation. Such pressure oscillations have been identified as a cause of cavitation in hydraulic rock drills, and the resulting erosion can lead to seal degradation [35]. The repeated impact contact at the piston end causes surface fatigue and material removal from the impact surface [36]. It is therefore necessary to examine the mechanism and condition of this secondary impact.

Before the secondary impact occurs, the piston and the load are in a state of equal velocity. This condition arises because, after the completion of Phase I, the stress distribution between the piston and the load becomes uniform, and the

two bodies share the same state of motion. This equal-velocity state is maintained throughout Phases II to IV until the onset of detachment and is governed by the contact force F_N between them. The equations of motion for the piston and the load can then be established, as shown in Eq.(28)

$$\begin{cases} m_p \ddot{x}_{p4} = -F_{pr} - F_N \\ \left(m_s + m_r\right)\ddot{x}_s = -k_L x_{p4} + F_{tt} + F_N \\ \ddot{x}_{p4} = \ddot{x}_s \end{cases} \tag{28}$$

where the F_{tt} is the thrust force of the hydraulic rock drill.

Therefore, the F_N can be given by Eq.(29)

$$F_N = \left[m_p k_L x_{p4} - \left(m_s + m_r\right) F_{pr} - m_p F_{pp} \right] / M \tag{29}$$

From Eq.(29), there exists a position at which the $F_N = 0$, indicating that the piston detaches from the load. If, at this moment, the rebound acceleration of the load exceeds that of the piston, a secondary impact may occur. Therefore, the critical position x_{dt} at which the piston detaches from the load can be obtained as Eq.(30)

$$x_{dt} = \frac{\left(m_s + m_r\right) F_{pr} + m_p F_{tt}}{m_p k_L} \tag{30}$$

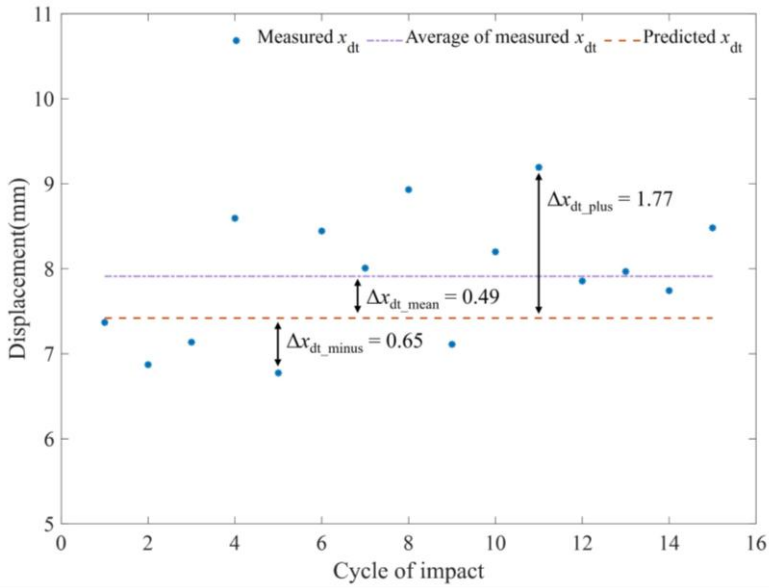


Figure 13 Comparison of the rebound detachment position and its mean position predicted by the proposed decomposition method

To validate the predicted detachment position, the experimental results under an operating pressure of 16 MPa are presented in Figure 13. The mean error is approximately 6.6%, with individual errors ranging from -8.8% to 23.9%. The mean error of 6.6% indicates that the proposed method is statistically accurate in predicting the detachment position, despite the occurrence of larger individual deviations. This discrepancy is attributed to the inherent variability of the hydraulic system during repeated impacts. Fluctuations in chamber pressure arise from oil leakage in the impacted cylinder during impact, while variations in oil temperature alter the effective bulk modulus of the hydraulic fluid. Both factors cause the load stiffness to deviate from its nominal value in certain impact cycles. Since these deviations are random and symmetrically distributed around the mean, they produce large individual errors while the average error remains low. Further improvement would require real-time characterization of these variations, which is beyond the scope of this study.

Despite these uncertainties, the detachment position prediction provides a practical basis for controlling the secondary

impact. The distance between the detachment position and the maximum compression moment determines the piston velocity at detachment, and thus the intensity of the secondary impact. This relationship identifies the thrust force as a key tuning parameter for mitigating secondary impact: by matching the thrust force so that the detachment position approaches the maximum compression position, the impact on the piston and seals can be effectively minimized.

5 Conclusion

This paper proposes a laser data-driven phase decomposition and dynamic modeling method for the transient impact process in percussive drilling. The method identifies the phase boundaries directly from measured piston displacement and establishes a phase-specific dynamic model that reconstructs the entire impact transient from measured data. The main conclusions and findings are summarized as follows:

(1) The phase boundaries of the impact process are identified from measured piston displacement using a jerk-based method. The boundaries are determined directly from the measured data and the known structural parameters of the rock drill, without relying on a predefined threshold or a manually specified phase interval. This provides a transferable basis for phase identification in systems where the impact position varies from cycle to cycle.

(2) A five-phase model of the impact process is established by combining the identified phase boundaries with the established phase-specific models. The model takes the initial impact velocity as input and predicts the piston velocity and the penetration depth during the impact process. The predicted piston velocity at the end of Phase I agrees with the measured value within 6.9%–8.5% under the lower stiffness condition and 0.9% under the higher stiffness condition, and the maximum penetration error is around 2%.

(3) The phase decomposition enables the energy partitioning between the transient impact phase and the subsequent compression phase to be calculated directly from the measured piston displacement. Under the tested conditions, lower load stiffness corresponds to a smaller kinetic energy loss at the end of Phase I and a larger penetration during Phases II–III, while higher load stiffness corresponds to the opposite. This indicates that the load stiffness governs how the impact energy is distributed between the transient impact phase and the subsequent compression phase, and this distribution directly influences the penetration.

(4) The detachment position of the piston during rebound can be predicted based on the proposed model. The distance between MCM and IOM_2 governs the intensity of the secondary impact, which can be adjusted by thrust force. This provides a basis for mitigating the secondary impact and reducing the fatigue loading on the piston and seal components.

In summary, the proposed method provides a reliable approach for characterizing the transient impact process of percussive drills, offering insights for performance optimization and durability improvement.

Funding declaration

This work was supported by the National Natural Science Foundation of China (Grant No. 52474171).

Competing interests

The authors declare that they have no competing interests.

Availability of data and materials

The datasets used and/or analysed during the current study are available from the corresponding author on reasonable request.

Reference

[1] Y. Li, P. Ranjith, Energy transition, mechanical response and rock fragmentation in percussion drilling: A review, Geoenergy Science and Engineering 250 (2025) 213838.

[2] H. Li, S. Liu, H. Chang, Experimental research on the influence of working parameters on the drilling efficiency, Tunnelling and underground space technology 95 (2020) 103174.

[3] J.R. Huerta, R.S. Silva, G. De Tomi, A.L.M. Ayres da Silva, A dynamic simulation approach to support operational decision-making in underground mining, Simulation Modelling Practice and Theory 115 (2022) 102458.
[4] S. Chang, M. Ye, D. Zhang, Y. Ma, J. Zhang, Impact performance optimization for hydraulic rock drill based on stroke and flow compensation factors, Advances in Mechanical Engineering 16 (6) (2024) 16878132241259579.
[5] L. Gorodilov, Mathematical models of hydraulic percussion systems, Journal of mining science 41 (5) (2005) 475–489.
[6] S. Yang, Y. Ou, Y. Guo, X. Wu, Analysis and optimization of the working parameters of the impact mechanism of hydraulic rock drill based on a numerical simulation, International Journal of Precision Engineering and Manufacturing 18 (7) (2017) 971–977.
[7] Q. Hu, C. Yang, H. Zheng, M. Chen, Dynamic simulation and test research of impact performance of hydraulic rock drill with no constant-pressurized chamber, Automation in Construction 37 (2014) 211–216.
[8] W. Ma, X. Geng, C. Jia, L. Gao, Y. Liu, X. Tian, Percussion characteristic analysis for hydraulic rock drill with no constant-pressurized chamber through numerical simulation and experiment, Advances in Mechanical Engineering 11 (4) (2019) 1687814019841486.
[9] B. Lundberg, P. Collet, Optimal wave shape with respect to efficiency in percussive drilling with detachable drill bit, International Journal of Impact Engineering 86 (2015) 179–187.
[10] B. Lundberg, T. Rastemo, J. Huo, Effect of pre-impact waves in an elastic rod on coefficient of restitution, International Journal of Impact Engineering 151 (2021) 103816.
[11] Y. Zhao, Y. Tang, W. Hou, X. Zeng, Influence of a waveform on the bit–rock impact response considering reflected waves in a drill rod, Computers and Geotechnics 173 (2024) 106572.
[12] K. Hashiba, T. Matsuda, Y. Yoshihara, K. Fukui, Force-penetration curves of a button bit generated during percussive rock drilling, International Journal of Rock Mechanics and Mining Sciences 183 (2024) 105925.
[13] H. Zhang, K. Liu, Z. Cai, Z. Dong, B. Yang, Y. Zhou, K. Lv, Study on damage characteristics of different types of rocks under stepped cyclic electrohydraulic shockwaves, Geoenergy Science and Engineering 250 (2025) 213810.
[14] Y. Zheng, Z. Su, J. Li, Z. Wang, Y. Xu, X. Li, P. Che, Energy transfer efficiency and rock damage characteristics of a hydraulic impact hammer with different tool shapes, International Journal of Impact Engineering 188 (2024) 104933.
[15] J. Huo, B. Lundberg, Realization of shorter substitutes for a percussive rock drill hammer by periodic redistribution of its mass and compliance, International Journal of Impact Engineering 180 (2023) 104725.
[16] D. Scaccabarozzi, B. Saggin, Measurement of stress waves propagation in percussive drilling, Sensors 21 (11) (2021) 3677.
[17] R. Yang, Y. Xu, P. Chen, J. Wang, Experimental study on dynamic mechanics and energy evolution of rubber concrete under cyclic impact loading and dynamic splitting tension, Construction and Building Materials 262 (2020) 120071.
[18] L. Cui, X. Zhang, H. Hao, Improved analysis for impact response prediction of reinforced concrete structures considering stress wave propagation and time dependent shape function, International Journal of Impact Engineering 182 (2023) 104783.
[19] Z. Watanabe, E. Yamada, On Electro-Magnetic Measurements of Rock Drill Performances, Journal of the Mining and Metallurgical Institute of Japan 80 (914) (1964) 665–668.
[20] Z. Yang, J. Li, G. Yu, Influence of piston mass and working pressure on the impact performance of a hydraulic rock drill using the stress wave method, Machines 11 (11) (2023) 987.
[21] Y. Li, Research on the matching of impact performance and collision coefficient of hydraulic rock drill, Shock and Vibration 1 (2021) 6651860.
[22] G. Guangfa, Stress wave effects and their mechanisms on stress-strain curves in the elastic phase of SHPB tests, International Journal of Impact Engineering 193 (2024) 105061.
[23] S. Goldman, H. Flashner, B. Yang, An approach to modeling percussive drilling systems, Journal of Vibration and Acoustics 144 (5) (2022) 051015.
[24] J. Li, Study on Compound Percussive Drilling: Rock-Breaking Mechanism of High Confining Pressure Formation in the East China Sea, Energy Science & Engineering 13 (7) (2025) 3688–3703.

[25] Z. Sun, Z. Huang, W. Zou, X. Wu, Z. Mu, X. Dai, X. Song, W. He, H. Chen, X. Li, Cracking behaviors of rocks subjected to the dynamic percussion of a single PDC cutter: a finite-discrete element study, Rock Mechanics and Rock Engineering 58 (3) (2025) 3039–3071.

[26] J.-D. Yu, J.-S. Lee, B. Tamang, S. Park, S. Chang, J. Kim, Y. Kim, Performance evaluation of GFRP rock bolt sensor for rock slope monitoring by double shear test, Advances in Civil Engineering 2020 (1) (2020) 8870698.

[27] X. Tian, W. Xi, F. Ma, Z. Zhang, S. Wang, X. Geng, Experimental study on impact coupling characteristics of high-pressure accumulator for unconstant-pressurized chamber rock drills, Advances in Mechanical Engineering 16 (10) (2024) 16878132241289264.

[28] J. Wang, P. Liang, Y. Zhang, X. Yao, G. Yu, Q. Han, Real-time identification of acoustic emission signals of rock tension-shear fracture based on machine learning and study on precursory characteristics, Mechanical Systems and Signal Processing 230 (2025) 112665.

[29] M. Qin, K. Wang, K. Pan, T. Sun, Z. Liu, Analysis of signal characteristics from rock drilling based on vibration and acoustic sensor approaches, Applied Acoustics 140 (2018) 275–282.

[30] M. Khoshouei, R. Bagherpour, M.H. Jalalian, Rock type identification using analysis of the acoustic signal frequency contents propagated while drilling operation, Geotechnical and Geological Engineering 40 (3) (2022) 1237–1250.

[31] W.A. Hustrulid, C. Fairhurst, A theoretical and experimental study of the percussive drilling of rock part I—theory of percussive drilling, International Journal of Rock Mechanics & Mining Sciences & Geomechanics Abstracts 8 (4) (1971) 311–333.

[32] B. Lundberg, J. Huo, Biconvex versus bilinear force-penetration relationship in percussive drilling of rock, International Journal of Impact Engineering 100 (2017) 7–12.

[33] B. Lundberg, Energy transfer in percussive rock destruction—I: Comparison of percussive methods, International Journal of Rock Mechanics & Mining Sciences & Geomechanics Abstracts 10 (5) (1973) 381–399.

[34] B. Lundberg, Microcomputer simulation of percussive drilling, International Journal of Rock Mechanics & Mining Sciences & Geomechanics Abstracts 22 (4) (1985) 237–249.

[35] X. Geng, W. Ma, F. Ma, Z. Zhou, Y. Liu, X. Tian, Cavitation erosion of the damping piston in double damping system of hydraulic rock drill and its influencing factors, AIP Advances 8 (11) (2018).

[36] R. Karimi Bakhshandi, A. Tkachuk, M. Sadek, J. Bergström, M. Grehk, Failure analysis of two cylindrical impact pistons subjected to high velocity impacts in drilling applications, Engineering Failure Analysis 140 (2022) 106623.